JACS
JOURNAL OF THE AMERICAN CHEMICAL SOCIETY

Communication

pubs.acs.org/JACS

Ultrathin Colloidal Cesium Lead Halide Perovskite Nanowires

Dandan Zhang,[†,§,⊥] Yi Yu,[†,§,⊥] Yehonadav Bekenstein,[†,§,∥,⊥] Andrew B. Wong,[†,§] A. Paul Alivisatos,[†,‡,§,∥] and Peidong Yang*[,†,‡,§,∥]

[†]Department of Chemistry, [‡]Department of Materials Science and Engineering, University of California, Berkeley, California 94720, United States

[§]Materials Sciences Division, Lawrence Berkeley National Laboratory, Berkeley, California 94720, United States

[∥]Kavli Energy NanoScience Institute, Berkeley, California 94720, United States

Supporting Information

ABSTRACT: Highly uniform single crystal ultrathin $CsPbBr_3$ nanowires (NWs) with diameter of 2.2 ± 0.2 nm and length up to several microns were successfully synthesized and purified using a catalyst-free colloidal synthesis method followed by a stepwise purification strategy. The NWs have bright photoluminescence (PL) with a photoluminescence quantum yield (PLQY) of about 30% after surface treatment. Large blue-shifted UV−vis absorption and PL spectra have been observed due to strong two-dimensional quantum confinement effects. A small angle X-ray scattering (SAXS) pattern shows the periodic packing of the ultrathin NWs along the radial direction, demonstrates the narrow radial distribution of the wires, and emphasizes the deep intercalation of the surfactants. Despite the extreme aspect ratios of the ultrathin NWs, their composition and the resulting optical properties can be readily tuned by an anion-exchange reaction with good morphology preservation. These bright ultrathin NWs may be used as a model system to study strong quantum confinement effects in a one-dimensional halide perovskite system.

Semiconductor nanowires (NWs) with an ultrathin diameter below the exciton Bohr radius, especially those with a diameter down to the atomic level (<3 nm), have attracted significant interest in the past few years because of their unique ability to combine the atomically thin radial dimension with the micron scale lengths. Moreover, their high surface area and their unique physical properties caused by strong quantum confinement effects position them as model systems to bridge and study the properties of nanomaterials and molecules.[1] Synthetically, it is a fundamental challenge to make uniform ultrathin NWs due to the increased difficulty to control crystal growth at the atomic level. So far, only limited kinds of ultrathin NWs have been reported, such as Au,[2] Ag,[3] Cu_2S,[4] Bi_2S_3,[5] CdS,[6] EuOF,[7] and ZnS.[8]

$CsPbX_3$ (X = Cl, Br, I) with the perovskite crystal structure is a class of important optoelectronic materials that have emerged in the past two years. The combination of its excellent optical and electronic properties and its promise for improved stability has implied it could be a robust alternative for hybrid lead halide perovskites, and it has already been used to demonstrate remarkable potentials in photovoltaics,[9] lasers,[10] and light emitting diode devices.[11] Following Protesescu et al. which established a reliable colloidal synthesis approach for $CsPbX_3$ nanocubes,[12] the morphological library has been rapidly extended to one-dimensional (1D) NWs[13] and two-dimensional (2D) nanoplates[14] by us and several other groups. However, unlike in the case of the 2D plates, currently the size of the NWs can only be controlled down to about 8 nm,[13b] which is on the borderline of its exciton Bohr radius, and it shows only weak exciton confinement.

In this communication, we develop a method to synthesize and purify highly uniform single-crystalline $CsPbBr_3$ NWs with diameters down to 2.2 ± 0.2 nm, which is well below the exciton Bohr radius of $CsPbBr_3$ (7 nm).[12] Large blue-shifted UV−vis absorption and photoluminescence (PL) spectra have been observed. The ultrathin NWs have bright photoluminescence with about a 30% photoluminescence quantum yield (PLQY) after purification and surface treatment. The diffraction pattern from small-angle X-ray scattering (SAXS) reflects the periodic packing of the ultrathin NWs, demonstrates the narrow size distribution of the NWs, and emphasizes the deep intercalation of the surfactants. Through anion-exchange reactions, the halide composition of the ultrathin NWs can be readily controlled with the preservation of the ultrathin NW morphology.

Colloidal synthesis of ultrathin $CsPbBr_3$ NWs was carried out using standard air-free techniques (Supporting Information (SI)). The yield of the ultrathin NWs is always low, only about several percent; thus, we developed a stepwise purification method to improve the purity of the sample to over 90%, by using different volumes of ethyl acetate (EA) as the antisolvent to gradually separate the ultrathin NWs from other impurities (Figure 1 and SI). Immediately following the synthesis, the solution was quenched by an ice−water bath and centrifuged to 6000 rpm for 5 min. The pelleted sample was discarded, and a certain amount of EA was added to the supernatant to precipitate the product. As shown in Figure 1, when 7 equiv of EA have been added to the supernatant, the product precipitated from the solution by centrifugation is mainly nanoparticles. The precipitated sample was separated from the supernatant, and a similar procedure utilized by adding more EA to the supernatant, until the third time, with the overall volume ratio of original supernatant to the antisolvent was

Received: August 10, 2016
Published: September 27, 2016

DOI: 10.1021/jacs.6b08373
J. Am. Chem. Soc. 2016, 138, 13155−13158

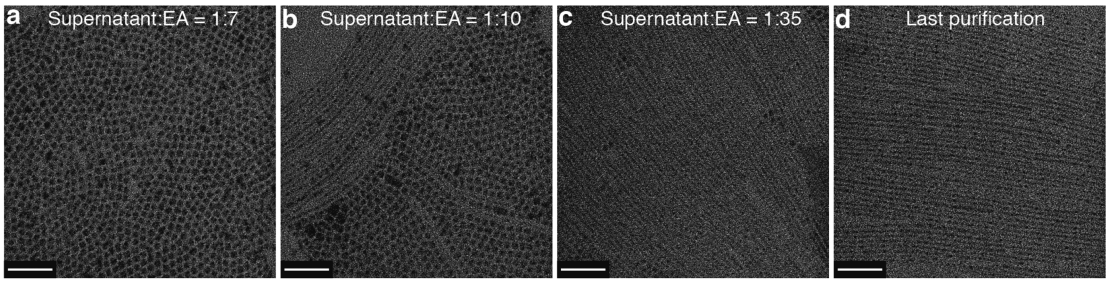

Figure 1. Stepwise purification process of ultrathin $CsPbBr_3$ NWs (scale bar: 50 nm).

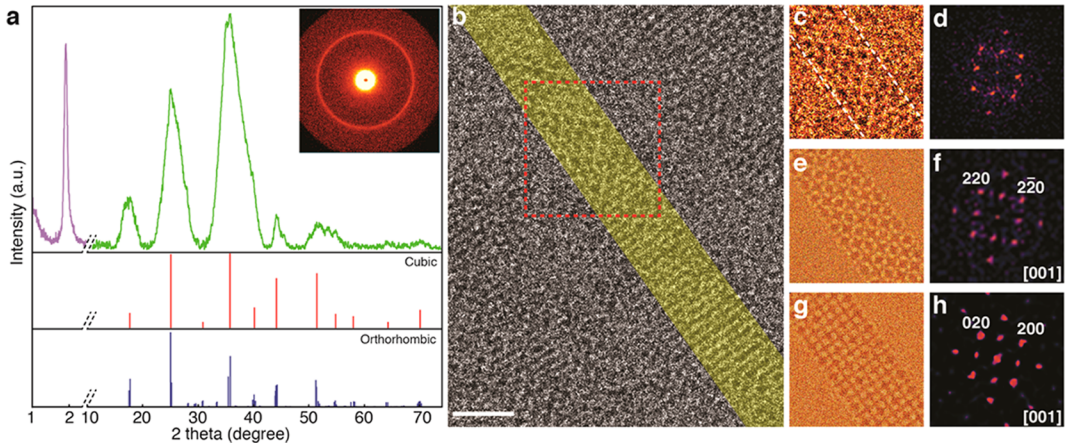

Figure 2. (a) Combined SAXS (purple) and XRD (green) experimental patterns recorded on the ultrathin $CsPbBr_3$ NWs, and the standard XRD patterns for cubic and orthorhombic phases of $CsPbBr_3$. The inset shows the corresponding SAXS pattern. (b) Experimental low dose AC-HRTEM image of a single ultrathin $CsPbBr_3$ NW. The dose rate is 48 $eÅ^{-2}$ s^{-1}, and the exposure time is 5 s, giving rise to a total dose of 240 $eÅ^{-2}$ within the single frame. False color is applied on the NW (scale bar: 2 nm). (c, d) False-colored image and corresponding diffractogram of the selected red-boxed region in (b). (e, f) Simulated AC-HRTEM image and corresponding diffractogram of orthorhombic $CsPbBr_3$ NW (Image defocus: −10 nm). (g, h) Simulated AC-HRTEM image and corresponding diffractogram of cubic $CsPbBr_3$ NW (Image defocus: −8 nm).

about 1:35, a relatively pure ultrathin NWs sample (>70% purity) can be achieved. However, the purification process can easily damage surface passivation of the nanomaterials by peeling off the binding ligands[15] and creating more surface states, which resulted in a relatively low quantum yield. And because of the high surface area of the ultrathin NWs, this effect severely affected the ultrathin NWs more so than the remaining nanocubes, so that even though ultrathin NWs are the major product in the sample as shown in Figure 1c, the PL spectrum of the same sample is still dominated by the residual nanocubes (Figure S1a). For optical characterizations, a final wash−centrifuge−redisperse purification cycle is necessary to further improve the purity of the ultrathin NWs to over 90% (Figure S1b). However, due to the fragile nature of the ultrathin NWs, extensive purification will inevitably induce some damage to the sample, such as increasing the size distribution and introducing a small amount of other undesirable morphologies (Figure S2). Therefore, for other structural characterizations, this final step was omitted to avoid further damage by additional purification steps. In general, the ultrathin NWs display remarkable diameter uniformity, but they will easily melt and become damaged after long-time electron beam irradiation. The corresponding energy dispersive X-ray spectroscopy (EDS) analysis (Figure S3) reveals that the NWs contain cesium, lead, and iodide, with a nearly 1.0:1.2:2.5 atomic ratio; this metal enrichment phenomenon is commonly observed in nanomaterials and known to increase with decreasing crystal size.[16] This effect is assigned to the fact that the ligands can preferentially bind to cationic metal ions, resulting in a metal-rich surface.

The transmission electron microscopy (TEM) image in Figure 1 shows that when the sample was dried on the TEM grid, the NWs tend to align parallel to each other and form closely packed highly ordered array structures. In order to characterize these structures, SAXS has been applied. As shown in Figure 2a, SAXS reflections show a prominent diffraction ring with a *d*-spacing of 4.63 nm, corresponding to the NW with a width of ∼2.2 nm plus two layers of surfactants with a large degree of intercalation (∼78%). The deep ligands intercalation explains why the wires tend to form bundles as shown in Figure S4. The full width at half-maximum (fwhm) of the diffraction peak is narrow and corresponds to 0.27 nm, indicating the remarkable diameter uniformity of the ultrathin NWs, which is consistent with the TEM observations. The SAXS pattern of the ultrathin NWs after final purification shows a larger *d*-spacing with wider fwhm (Figure S2), which is due to the damage of the NWs caused by extensive washing as discussed above.

The standard powder X-ray diffraction (XRD) patterns of cubic and orthorhombic $CsPbBr_3$ phases can both fit the experimental XRD of the ultrathin NWs (Figure 2a); the severe peak broadening due to the small size of the NWs prevents the unequivocal determination of their crystal structure. High-resolution TEM (HRTEM) has been performed to further characterize the structure of the ultrathin $CsPbBr_3$ NWs. However, HRTEM images of the $CsPbBr_3$ ultrathin NWs have

DOI: 10.1021/jacs.6b08373
J. Am. Chem. Soc. 2016, 138, 13155−13158

proven exceptionally challenging to acquire because they are sensitive to beam damage, and their small size can only provide limited image contrast. In order to resolve those problems, we use aberration-corrected HRTEM (AC-HRTEM), which can improve the image resolution by minimizing the surface delocalization effect.[17] Also, we carefully control the imaging electron dose to minimize the beam damage. The electron doses were chosen such that the pristine crystal structure could be maintained during the image acquisition. Figure 2b shows a low-dose AC-HRTEM image of a single $CsPbBr_3$ NW with ~2.2 nm in diameter. The well-resolved lattice image in the red-boxed region and the corresponding diffractogram are shown in Figure 2c and 2d, indicating the single-crystalline feature of the ultrathin NWs. To further analyze the structure, image simulations were carried out. Figure 3e–3h show the simulated images and the corresponding diffractograms of orthorhombic and cubic phase $CsPbBr_3$ NWs, respectively. Qualitatively, both the orthorhombic- and cubic-phase simulations can fit well with our experimental result because of the highly similar characteristics between those two phases. As a result, it is still quite difficult to unequivocally determine the crystal structure of the ultrathin NWs even with the combination of high-resolution imaging and simulations. In order to obtain a complete and reliable model of the structure of the ultrathin NWs, complementary structural characterization techniques such as X-ray absorption spectroscopy (XAS), Raman spectroscopy, and nuclear magnetic resonance (NMR) may be needed for future work.

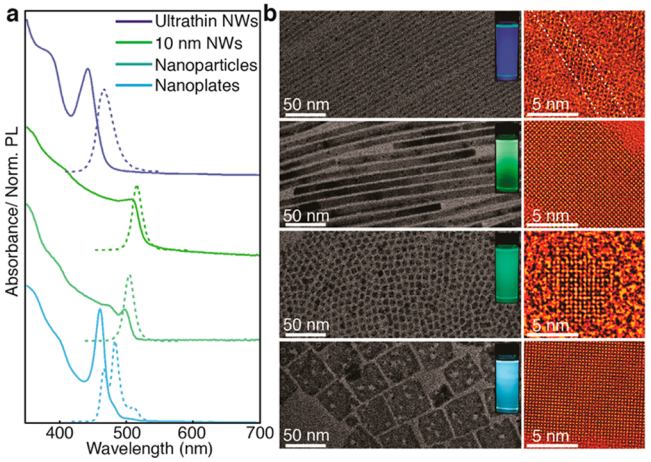

Figure 3. (a) Optical absorption (solid line) and PL (dash line) spectra. (b) Low-resolution TEM and AC-HRTEM images of $CsPbBr_3$ ultrathin NWs, 10 ± 2 nm NWs, nanocrystals, and nanoplates. The insets show the emission color of different morphological species under UV illumination (λ = 365 nm).

In order to restore the surface passivation of the NWs and improve the QY, surface treatment with $PbBr_2$ precursor was performed (SI). PLQY measurement shows that the QY of the ultrathin NWs is around 30% (Figure S5), which is lower than the QY of our previously reported 10 nm $CsPbBr_3$ NWs (PLQY = 53%),[13b] which is probably due to the increased surface states. Notably, the surface treatment can not only increase the QY of the ultrathin NWs but also improve the stability of the NWs by retarding its ripening processes. An example of this is demonstrated in Figure S6, where the NWs were drop casted on TEM grids and stored in a desiccator. Samples without surface treatment will break and ripen in 3 days, while the one with surface treatment will be stable for weeks. When dispersed in solution, the ultrathin NWs will gradually ripen to form larger wires and crystals (Figure S7).

To inspect the quantum confinement effect of the ultrathin NWs, UV–vis absorption and PL spectra were measured. As shown in Figure 3, the solution of the ultrathin NWs shows bright blue emission under a UV-lamp. The distinct peak at λ = 442 nm (2.81 eV) in the UV–vis absorption spectrum is due to the first absorption band of the ultrathin NWs; the sharp absorption peak also indicates that the NWs are uniform in diameter, which is consistent with the TEM results. The PL emission spectrum exhibits a relatively narrow peak centered at λ = 465 nm (2.67 eV) with an fwhm of 0.15 eV and a typical Stokes shift of 0.14 eV. The blue-shifted emission compared to that of the nanocrystals, nanoplates, and 10-nm-thick NWs indicates the existence of a very strong two-dimensional quantum confinement effect. And the larger Stokes shift in the ultrathin NWs implies that the band-edge electronic structure of $CsPbBr_3$ is highly size dependent. The peak position is in close agreement with the emission of the 4-unit-cell thick $CsPbBr_3$ (2.33 nm) nanoplates,[14a] and considering this is the sample after final purification, then the original wires should have even smaller diameters, which are in accordance with TEM and SAXS observations.

In order to achieve wide chemical tunability, a facial anion-exchange process has been applied to the ultrathin $CsPbBr_3$ NWs in which Br^- anions are replaced with either Cl^- or I^- ions. Halide-exchange reactions were carried out at room temperature using PbX_2 (X = Cl, I) as precursors (SI). The

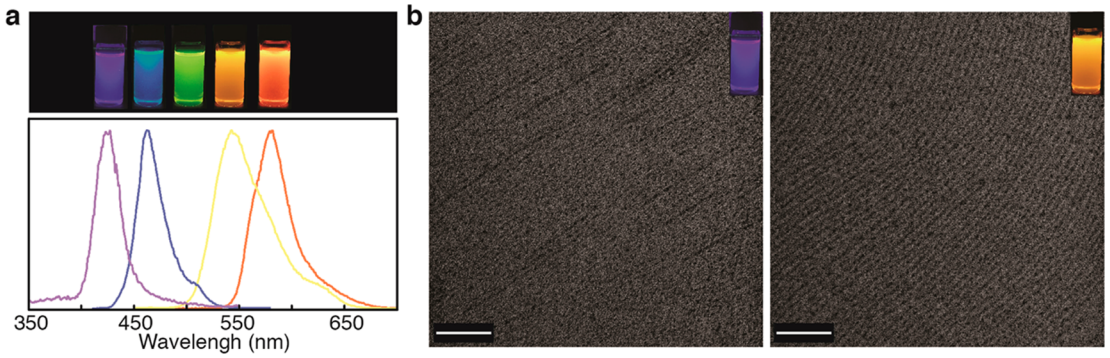

Figure 4. (a) Colloidal solution of anion-exchanged ultrathin NWs in toluene under UV illumination (λ = 365 nm). Corresponding PL spectra of the halide-anion exchanged samples. (b) TEM images of Cl- and I-exchange NWs (scale bar: 50 nm).

DOI: 10.1021/jacs.6b08373
J. Am. Chem. Soc. 2016, 138, 13155–13158

blue emission from the ultrathin $CsPbBr_3$ NWs can be readily tuned through purple to red emission with a different conversion degree, and surprisingly the morphology of the ultrathin wires have been largely preserved. The slightly size expansion (Br−I exchange) and contraction (Br−Cl exchange) can also be readily observed from the TEM images (Figures 4 and S8). It is worth mentioning that when an excess amount of anion-exchange precursor has been add into the system, a competitive reaction mechanism other than an anion-exchange reaction can be clearly observed, involving damage to the ultrathin NWs with the formation of nanocubes and irregular nanocrystals (Figure S9). We suspect that coordinating an excessive amount of ligands on the ultrathin wires will gradually etch and dissolve the NWs, subsequently leading to formation of other morphologies, such as cubes or irregular crystals, which are thermodynamically more favorable. This undesirable competitive reaction can be largely suppressed by reducing the amount of the precursor. However, occasionally asymmetric red emission tails observed in the PL emission spectra (Figure 4a) implies that a small portion of the ultrathin NWs are still damaged during the anion-exchange process.

The exact mechanism of the growth of ultrathin $CsPbBr_3$ NWs is still largely unknown. The presence of particles with a larger size than the diameter of the NWs disfavors an oriented attachment mechanism. And an *in situ* aliquots study is not suitable, due to the coexistence of other morphological species. During the revision of this manuscript, Imran et al. demonstrated the role of ligands in controlling the diameter of perovskite NWs.[18] This along with previous reports[14b,19] suggests a complicated kinetically driven growth process for lower dimensionality perovskites, for which the details are not fully understood, demanding further investigation.

In conclusion, we have developed a method to synthesize and purify ultrathin $CsPbBr_3$ NWs with a uniform diameter of 2.2 ± 0.2 nm. Structural characterization techniques such as AC-HRTEM show the NWs are single crystalline. The combination of strong two-dimensional quantum confinement effects along with bright emission and band gap tunability positions these ultrathin NWs as a unique model system for the study of strong quantum confinement effects in one-dimensional halide perovskites.

■ ASSOCIATED CONTENT

Supporting Information

The Supporting Information is available free of charge on the ACS Publications website at DOI: 10.1021/jacs.6b08373.

Experimental details, additional UV/vis, PL, TEM, SAXS, EDS, PLQY (PDF)

■ AUTHOR INFORMATION

Corresponding Author

*p_yang@berkeley.edu

Author Contributions

⊥D.Z., Y.Y., and Y.B. contributed equally to this work.

Notes

The authors declare no competing financial interest.

■ ACKNOWLEDGMENTS

This work was supported by the Physical Chemistry of Inorganic Nanostructures Program, KC3103, Office of Basic Energy Sciences of the United States Department of Energy under Contract No. DE-AC02-05CH11231. Work at the NCEM, Molecular Foundry was supported by the Office of Science, Office of Basic Energy Sciences of the U.S. Department of Energy under Contract No. DE-AC02-05CH11231. D.Z. would like to acknowledge the fellowship support from Suzhou Industrial Park. A.B.W. would like to acknowledge the support of the LAM Research Fellowship.

■ REFERENCES

(1) Cademartiri, L.; Ozin, G. A. *Adv. Mater.* **2009**, *21*, 1013.

(2) (a) Huo, Z.; Tsung, C.-k.; Huang, W.; Zhang, X.; Yang, P. *Nano Lett.* **2008**, *8*, 2041. (b) Lu, X.; Yavuz, M. S.; Tuan, H.-Y.; Korgel, B. A.; Xia, Y. *J. Am. Chem. Soc.* **2008**, *130*, 8900.

(3) Hong, B. H.; Bae, S. C.; Lee, C.-W.; Jeong, S.; Kim, K. S. *Science* **2001**, *294*, 348.

(4) Liu, Z.; Xu, D.; Liang, J.; Shen, J.; Zhang, S.; Qian, Y. *J. Phys. Chem. B* **2005**, *109*, 10699.

(5) Thomson, J. W.; Cademartiri, L.; MacDonald, M.; Petrov, S.; Calestani, G.; Zhang, P.; Ozin, G. A. *J. Am. Chem. Soc.* **2010**, *132*, 9058.

(6) Zhuang, Z.; Lu, X.; Peng, Q.; Li, Y. *J. Am. Chem. Soc.* **2010**, *132*, 1819.

(7) Du, Y.-P.; Zhang, Y.-W.; Yan, Z.-G.; Sun, L.-D.; Yan, C.-H. *J. Am. Chem. Soc.* **2009**, *131*, 16364.

(8) Zhu, G.; Zhang, S.; Xu, Z.; Ma, J.; Shen, X. *J. Am. Chem. Soc.* **2011**, *133*, 15605.

(9) Kulbak, M.; Cahen, D.; Hodes, G. *J. Phys. Chem. Lett.* **2015**, *6*, 2452.

(10) Eaton, S. W.; Lai, M.; Gibson, N. A.; Wong, A. B.; Dou, L.; Ma, J.; Wang, L. W.; Leone, S. R.; Yang, P. *Proc. Natl. Acad. Sci. U. S. A.* **2016**, *113*, 1993.

(11) Yantara, N.; Bhaumik, S.; Yan, F.; Sabba, D.; Dewi, H. A.; Mathews, N.; Boix, P. P.; Demir, H. V.; Mhaisalkar, S. *J. Phys. Chem. Lett.* **2015**, *6*, 4360.

(12) Protesescu, L.; Yakunin, S.; Bodnarchuk, M. I.; Krieg, F.; Caputo, R.; Hendon, C. H.; Yang, R. X.; Walsh, A.; Kovalenko, M. V. *Nano Lett.* **2015**, *15*, 3692.

(13) (a) Zhang, D.; Eaton, S. W.; Yu, Y.; Dou, L.; Yang, P. *J. Am. Chem. Soc.* **2015**, *137*, 9230. (b) Zhang, D.; Yang, Y.; Bekenstein, Y.; Yu, Y.; Gibson, N. A.; Wong, A. B.; Eaton, S. W.; Kornienko, N.; Kong, Q.; Lai, M.; Alivisatos, A. P.; Leone, S. R.; Yang, P. *J. Am. Chem. Soc.* **2016**, *138*, 7236.

(14) (a) Bekenstein, Y.; Koscher, B. A.; Eaton, S. W.; Yang, P.; Alivisatos, A. P. *J. Am. Chem. Soc.* **2015**, *137*, 16008. (b) Shamsi, J.; Dang, Z.; Bianchini, P.; Canale, C.; Stasio, F. D.; Brescia, R.; Prato, M.; Manna, L. *J. Am. Chem. Soc.* **2016**, *138*, 7240. (c) Akkerman, Q. A.; Motti, S. G.; Srimath Kandada, A. R.; Mosconi, E.; D'Innocenzo, V.; Bertoni, G.; Marras, S.; Kamino, B. A.; Miranda, L.; De Angelis, F.; Petrozza, A.; Prato, M.; Manna, L. *J. Am. Chem. Soc.* **2016**, *138*, 1010.

(15) De Roo, J.; Ibanez, M.; Geiregat, P.; Nedelcu, G.; Walravens, W.; Maes, J.; Martins, J. C.; Van Driessche, I.; Kovalenko, M. V.; Hens, Z. *ACS Nano* **2016**, *10*, 2071.

(16) Anderson, N. C.; Hendricks, M. P.; Choi, J. J.; Owen, J. S. *J. Am. Chem. Soc.* **2013**, *135*, 18536.

(17) (a) Urban, K. W. *Science* **2008**, *321*, 506. (b) Yu, Y.; Cui, F.; Sun, J.; Yang, P. *Nano Lett.* **2016**, *16*, 3078.

(18) Imran, M.; Di Stasio, F.; Dang, Z.; Canale, C.; Khan, A. H.; Shamsi, J.; Brescia, R.; Prato, M.; Manna, L. *Chem. Mater.* **2016**, DOI: 10.1021/acs.chemmater.6b03081.

(19) Pan, A.; He, B.; Fan, X.; Liu, Z.; Urban, J. J.; Alivisatos, A. P.; He, L.; Liu, Y. *ACS Nano* **2016**, *10*, 7943.

DOI: 10.1021/jacs.6b08373
J. Am. Chem. Soc. 2016, 138, 13155−13158